

Irreducible QCD backgrounds to top searches in semi-leptonic final states at the Next Linear Collider

S. Moretti

*Rutherford Appleton Laboratory,
Chilton, Didcot, Oxon OX11 0QX, UK.*

Abstract

At future electron-positron colliders, one of the largest irreducible backgrounds to top searches in the channel '4 jets + lepton + missing energy' comes from QCD events of order α_s^2 . We compute here such processes exactly at the parton level by resorting to $2 \rightarrow 6$ matrix elements exploiting helicity amplitude techniques. We adopt a typical selection procedure based on the tagging of a high momentum and separated lepton. We finally outline kinematic differences between signal and background events that can be exploited to further reduce such a QCD noise.

1 Introduction

One of the *top* on the list reasons to build an e^+e^- linear collider (NLC) with a centre-of-mass (CM) energy between 350 and 1 TeV [1] is to study in great detail the *top* parameters: its mass (m_t), width (Γ_t), quantum numbers (Q_t, I_t^3) and branching ratios (BRs) [2]. Not surprisingly so, as it is not unreasonable to believe that the heaviest of the fundamental particles discovered so far would after all have something to teach us [3]. Indeed, in the unforeseen scenario that no Higgs bosons and no Supersymmetric (SUSY) particles are found at the LHC [4], this might even be the only task left for the NLC: to run as a top factory¹. Needless to say, under such a gloomy prospect, one would want to make the most out of such a machine, one way or another.

Our contribution in that respect is to calculate the $2 \rightarrow 6$ scattering processes

$$e^+e^- \rightarrow q\bar{q} Q\bar{Q}' \ell\nu_\ell \quad (1)$$

$$e^+e^- \rightarrow gg Q\bar{Q}' \ell\nu_\ell \quad (2)$$

at the parton level, through the perturbative order $\mathcal{O}(\alpha_{em}^4 \alpha_s^2)$, for any possible flavour combination of quarks $q, Q, Q' = u, \dots, b \neq t$ and leptons ℓ, ν_ℓ , with $\ell = e, \mu \neq \tau$. The sum of these two mechanisms represents one of the largest ‘irreducible’ backgrounds to top production and decay in the semileptonic channel

$$e^+e^- \rightarrow t\bar{t} \rightarrow b\bar{b} Q\bar{Q}' \ell\nu_\ell, \quad (3)$$

the one preferred for experimental studies [5]. Their calculation has never been attempted before². Obviously, if one wants to perform precision measurements of top parameters at the NLC, to pin down the size and shape of all important background processes is of paramount importance.

The plan of the paper is as follows. Next Section describes our calculations. The third one presents our results. Conclusions are in Sect. 4.

2 Calculation

Most of the Feynman diagrams that one has to tackle in order to calculate processes (1)–(2) proceed through $W^{\pm*} + 4$ jet production [6], with the gauge bosons subsequently decaying to lepton-neutrino pairs, see first four(six) graphs in Fig. 1(2). In addition to these, one also has to consider the graphs in which the off-shell $W^{\pm*}$ boson is produced in the bremsstrahlung off a leptonic current, see the last one(two) in Fig. 1(2), and eventually decays to four partons. Altogether one has to compute 140 diagrams: 32 associated with process (1) and 108 with (2). (Notice that for the time being we neglect diagrams in which an electron

¹The other, more frightening legacy of a Higgs- and SUSY-less LHC would be a strongly interactive weak sector, building up somewhere around the TeV scale, the very upper end of, if not beyond, the technical reach of the NLC as well as of many perturbative calculations !

²A preliminary exercise in such direction was performed in [6], where however only the case of on-shell W^\pm production plus four jets was considered. For the case of $\mathcal{O}(\alpha_{em}^6)$ backgrounds see Ref. [7].

and the companion neutrino in the final states of (1)–(2), i.e., $\ell = e$, are connected to the incoming beams via so-called ‘multi-peripheral’ channels. We will come back to this point in the conclusive Section.) The signal comes via two simple s -channel graphs (that we do not reproduce here).

We calculate the signal (3) at the leading-order (LO), though we are aware that several higher order electroweak and QCD corrections (mainly to the on-shell production) are known to date [3, 8]. We do this for consistency, as the background processes (1)–(2) can only be evaluated at tree-level with present technology. To compute all graphs is not a prohibitive task, if one resorts to helicity amplitudes methods. We have done so, by using both MadGraph [9] and a self-made program based on the technique of Ref. [10]. They agree with each other. Moreover, they have passed all our gauge-invariance tests, so to give us confidence in our numerical results.

To obtain the latter, one has to integrate the Feynman amplitudes squared over a six-body phase space. This task is not difficult either, provided one takes some special care in dealing with the various resonances. To get around this problem we have proceeded as described in Ref. [11]. That is, by splitting the gauge-invariant matrix elements of (1)–(2) in several sub-terms, each having its peculiar resonant structure. To any of these a dedicated mapping of the phase space has been attributed. These pieces have eventually been summed up together, after integration (performed with different packages, for cross-check purposes), so to recover gauge-invariance. A flat phase space has been instead used to integrate the interferences between the different sub-terms, with the help of some brute force too (i.e., a largely increased number of random calls). In general, we have verified that their contribution is never dominant, but not necessarily negligible, as compared to the pure resonances. For reason of space, we will not dwell here in technicalities any further, as we will discuss only the total integrated rates, summed over all production sub-channels.

Before proceeding to present our results, we list the numerical values adopted for the various Standard Model parameters:

$$\begin{aligned}
m_\ell &= m_{\nu_\ell} = m_u = m_d = m_s = m_c = 0, \\
m_b &= 4.25 \text{ GeV}, & m_t &= 175 \text{ GeV}, \\
M_Z &= 91.175 \text{ GeV}, & \Gamma_Z &= 2.5 \text{ GeV}, \\
M_W &= 80.23 \text{ GeV}, & \Gamma_W &= 2.08 \text{ GeV}.
\end{aligned}$$

As for the top width Γ_t , we have used the leading-order (LO) value of 1.55 GeV as a default. However, in a few cases, we have compared the yield of process (3) with finite width effects to that of the same reaction in Narrow Width Approximation (NWA), for which we have rewritten the (denominator of the) top quark propagator as

$$\frac{1}{p^2 - m_t^2 + im_t\Gamma} \left(\frac{\Gamma}{\Gamma_t} \right)^{1/2}, \tag{4}$$

with $\Gamma \rightarrow 0$, thus mimicking a delta function³ $\delta(p^2 - m_t^2)$.

³For $\Gamma \lesssim 10^{-5}$ GeV the total cross sections in NWA are stable and reproduce the on-shell results of the $2 \rightarrow 2$ process $e^+e^- \rightarrow t\bar{t}$ within numerical accuracy. (Note that for $\Gamma \equiv \Gamma_t$ in eq. (4) the standard expression of the propagator is recovered.)

For the vector and axial couplings of the gauge bosons to the fermions, we use the ‘effective leptonic’ value

$$\sin^2(\theta_W) \equiv \sin_{\text{eff}}^2(\theta_W) = 0.2320. \quad (5)$$

The strong coupling constant α_s entering processes (1)–(2) has been evaluated at two loops, with $N_f = 5$ and $\Lambda_{\overline{\text{MS}}} = 200$ MeV, at the scale $Q^2 = s$. The electromagnetic one was set at $1/128$. Finally, the centre-of-mass (CM) energies considered for the NLC are $\sqrt{s} \equiv E_{\text{cm}} = 360$ and 500 GeV, as representative of the threshold, $\sqrt{s} \gtrsim 2m_t$, and asymptotic, $\sqrt{s} \gg 2m_t$, top-antitop production regimes. Beyond those energies is no longer the top quark realm.

3 Results

In discussing the interplay between the background (1)–(2) and signal (3) processes, we have focused our attention to the case of the semi-leptonic (or, equivalently, semi-hadronic) signature

$$4 \text{ jets} + \ell^\pm + \cancel{E}, \quad (6)$$

where $\ell = e$ or μ , \cancel{E} represents the missing energy/momentum due to the neutrino ν_ℓ escaping detection and where to the four-jet hadronic system no b -tagging is applied⁴. We identify the quarks and gluons in (1)–(3) with the jets in (6) and apply all our cuts directly at the partonic level.

The choice of considering here only the final state (6) is indeed not restrictive, in the sense that the latter is to date the experimentally preferred channel in searching for $e^+e^- \rightarrow t\bar{t} \rightarrow b\bar{b}W^+W^-$ events. On the one hand, as opposed to the fully hadronic signature $b\bar{b}W^+W^- \rightarrow 6$ jets, it has a simpler detector topology and thus is much easier to reconstruct, further allowing one to reduce the severe problems due to the six-jet combinatorics (particularly, if no heavy quark identification is exploited)⁵. On the other hand, the case involving two leptonic W^\pm decays has a double disadvantage as compared to channel (6), that is, a very much reduced statistics and problems in reconstructing the top mass spectra because of the two neutrinos. Furthermore, as selection method of candidate top-antitop events we adopt one rather similar to that outlined in Sect. 4.2 of Ref. [5], based on the detection of high-momentum isolated leptons. As a matter of fact, such a procedure has been shown to be the most effective one, as it eventually yields the largest signal-to-background ratio, both at and above threshold: see Tab. 4.2 of [5].

About 40% of top-antitop events (3) produce an energetic electron or muon which is clearly separated from the hadronic system. Following Ref. [5], we consider a lepton to be isolated if a jet clustering algorithm with a ‘minimum mass’ cut-off recognises it as a ‘jet’ with a single particle. As jet finder we use the Jade one [12], with $y > 0.003(0.002)$ at $\sqrt{s} = 360(500)$ GeV, so that $M_{\ell^\pm j} \equiv 2E_{\ell^\pm}E_j(1 - \cos\theta_{\ell^\pm j}) > 19(22)$ GeV for each jet j in

⁴If the latter is enforced, we have already shown in Ref. [6] that the irreducible background to top events due to ‘ $W^\pm + 2 b + 2$ jet’ events is negligible, provided that a vertex tagging efficiency $\epsilon_b \gtrsim 0.5$ can be achieved.

⁵Also notice that, once the missing energy/momentum has been assigned to the neutrino, the kinematics of (6) is fully constrained, like in the case of the purely hadronic channel.

(6). As the MEs of the background processes are divergent if the partons are allowed to be infinitely soft and/or collinear, we also apply the jet clustering algorithm to the hadronic part of the event, for all cases (1)–(3). Fig. 3 presents the y -dependent total rates for these three processes as obtained by enforcing the jet clustering algorithm only, e.g., at $\sqrt{s} = 360$ GeV. Notice that there exists a hierarchy in the production rates:

$$\sigma(e^+e^- \rightarrow t\bar{t} \rightarrow b\bar{b} Q\bar{Q}' \ell\nu_\ell) \gg \sigma(e^+e^- \rightarrow gg Q\bar{Q}' \ell\nu_\ell) \gg \sigma(e^+e^- \rightarrow q\bar{q} Q\bar{Q}' \ell\nu_\ell). \quad (7)$$

At the minimum value of y considered here, they approximately scale as 100:10:1. If $\sqrt{s} = 500$ GeV, see Fig. 4, the relative ratio of process (3) to either of (2) or (1) further increases, while that between the latter two suffers little from the CM energy scaling. As for top width effects, whereas these are naturally sizable at threshold (with differences of about 10%, see the top-right insert in Fig. 3), they instead fall to the percent level in the asymptotic regime (Fig. 4) [13].

In Figs. 3–4 we have neglected considering Initial State Radiation (ISR) [14], that is, the presence of bremsstrahlung photons emitted by the incoming electron/positron beams⁶. The main consequence of ISR is to lower the effective CM energy, thus ultimately reducing(enhancing) the production rates of processes whose cross sections increase(decrease) with \sqrt{s} . One thus expects the top-antitop rates (3) to be rather sensitive to ISR, for two reasons. Firstly, because of the s -channel topology of the Feynman diagrams involved (which tends to increase the rates). Secondly, at threshold, because the difference $\sqrt{s} - 2m_t$ starts approaching the edge of the phase space (thus decreasing the rates). In contrast, the background rates (1)–(2) should depend much less on the ISR. On the one hand, they are not purely s -channel. On the other hand, \sqrt{s} is well above the heavy particle thresholds which can onset there (such as the dominant W^+W^-).

This dynamics can be appreciated by comparing the total cross sections in the upper lines of Tab. 1, when no selection cuts are applied apart from the jet clustering algorithm. There, notice that the background rates (third and fourth column) outside and inside brackets are rather steady, at both collider energies. For signal events, both in NWA and with finite top width (first and second column), differences are much more sizable. At threshold, it is clearly the phase space suppression to dominate, depleting the signal rates by up to 43% (at the minimum y). In the asymptotic regime, where phase space effects become negligible, the s -channel increase is overturned by the presence of the invariant mass constraints, as also typical energies of the final state particles diminish because of ISR.

Indeed, in presence of the latter, the response of processes (1)–(3) to the implementation of any selection cuts is no longer straightforward, as a consequence of the fact that ISR also induces a smearing of the differential distributions. Thus, from now onwards, all our results will include initial state bremsstrahlung. (We will keep those without it only for reference purposes.) Among the various ways of implementing the ISR, we have adopted here the so-called Electron Structure Function (ESF) approach, based on the formulae given in Ref. [15]. In addition, hereafter, we will stop considering the case of process (3) in NWA.

⁶Also beamsstrahlung and Linac energy spread [14] in principle affect processes (1)–(3). In practise, for narrow beam designs of the NLC, their effects are much smaller as compared to those induced by ISR [14], so for the time being we neglect the former in our analysis.

We now proceed by applying all other selection cuts of [5] that can be exploited at parton level too. Namely, an event is accepted if:

1. its ‘thrust’ (calculated by using the four jet and the lepton momenta), $T_{\ell^\pm, j}$, is significantly far from the infrared region typical of QCD events;
2. the invariant mass of the hadronic system, M_{4j} , is far above the typical resonances of background events (M_W in our case);
3. the amount of missing energy, \cancel{E} , is rather contained, as in top events this is typically less than $\sqrt{m_t^2 - M_W^2}$;
4. the (absolute) momentum of the isolated lepton, $|\vec{p}_{\ell^\pm}|$, is above a minimum energy threshold and below a maximum one of standard acceptance.

Numerically, to account for other sources of background too, other than (1)–(2), we require [5]:

$$\begin{aligned} T_{\ell^\pm, j} &< 0.75 & M_{4j} &> 0.4\sqrt{s} \\ \cancel{E} &< 0.4\sqrt{s} & 0.04\sqrt{s} &< |\vec{p}_{\ell^\pm}| < 0.3\sqrt{s}. \end{aligned} \quad (8)$$

The second line in Tab. 1 reports our findings. After the cuts in (8) are enforced, the background from processes (1)–(2) amounts to about 1.6% of the signal (3) at threshold, whereas well above that the corresponding figure is $\approx 0.9\%$. Thus, in both cases, the QCD noise is under control.

Nonetheless, one ought to know its effects on the differential spectra used to fit the top parameters. We consider here all possible three-jet mass distributions M_{ijk} which can be reconstructed in samples of the type (6). After ordering the four jets in energy, such that $E_1 > \dots > E_4$, one can build up four ijk combinations, such that $i < j < k$. They are presented in Figs. 5 and 6, for the cases $\sqrt{s} = 360$ and 500 GeV, respectively. The size and shape of the backgrounds (1)–(2) are rather innocuous in the vicinity of the top peaks, so that one should not expect any significant distortion of the Breit-Wigner distribution of the top resonances. As a matter of fact, in this respect, it is the intrinsic background due to mis-assigned jets originating in the signal (3) from b -quarks that affects most the signal, as discussed in Refs. [11, 13].

Finally notice that an additional requirement can be imposed to events of the form (6), in order to increase the signal-to-background ratio of (3) vs. (1)–(2). That is, that one two-jet combination ij , among the six possible possible ones, when $i < j = 1, \dots, 4$, produces an invariant mass M_{ij} around the W^\pm mass. As one can appreciate in Figs. 7–8, this would reduce the QCD noise to imperceptible levels. If one imposes at $\sqrt{s} = 360$ GeV, e.g., $|M_{34} - M_W| \leq 20$ GeV, then additional reduction factors of 9.1 and 8.4 apply to the processes (1) and (2), respectively, whereas the loss on the signal (3) is just 1.3. Corresponding numbers at $\sqrt{s} = 500$ GeV are 4.3 and 3.7 for the backgrounds, and 1.6 for the signal. Finally, we should mention that we have tried other quantities too (such as, e.g., jet energies, relative angles, etc.) but they have proved themselves much less useful than the M_{ij} spectra in disentangling reactions (1)–(2) and (3).

4 Conclusions

Thus we conclude that irreducible $\mathcal{O}(\alpha_{em}^4 \alpha_s^2)$ backgrounds to the ‘4 jets + lepton + missing energy’ signature of top-antitop events at the Next Linear Collider are reduced at the ten percent level by using a standard selection procedure (at typical design energies), in line with previous results obtained by using parton shower models. Such figure can vigorously be reduced further if a simple mass requirement on a two-jet system is imposed. We have obtained such results by computing tree-level matrix elements at leading-order for the relevant $2 \rightarrow 6$ processes, with the only exception of multi-peripheral graphs entering final states including electrons. We have neglected the latter for two reasons. On the one hand, we would have had to calculate twice as many diagrams as compared to the way we did it. On the other hand, the contributions of the missing terms has already been proved to be very small in the case of $\mathcal{O}(\alpha_{em}^6) e^+e^- \rightarrow b\bar{b} Q\bar{Q}' \ell\nu_\ell$ processes, as their inclusion account for an increase of only 6% with respect to the muon rates, for a CM energy of 500 GeV [7]. Indeed, we expect the same to have occurred here. Anyhow, given the results we have eventually obtained for the signal-to-background ratio, even if their rate is actually much larger than the mentioned figure, our conclusions would remain unchanged. Finally, we believe that, although confined at the partonic stage, our findings should not be invalidated by studies at the hadronic level. We make our programs available to the public for simulation purposes in the above respect.

Acknowledgements

We thank the Department of Theoretical Physics of Granada University for the kind hospitality while this project was conceived and Ramon Muñoz-Tapia for discussions. Financial support is provided by the UK PPARC.

References

- [1] Proceedings of the Workshop “ e^+e^- Collisions at 500 GeV. The Physics Potential”, Munich, Annecy, Hamburg, 3–4 February 1991, ed. P.M. Zerwas, DESY 92–123A/B, August 1992, DESY 93–123C, December 1993.
- [2] See, e.g.:
Section ‘Top Quark Physics’, P. Igo-Kemenes and J.H. Kühn conveners, in Ref. [1] (and references therein), part A.
- [3] W. Bernreuther *et al.*, in Ref. [1], part A.
- [4] CMS Technical Proposal, CERN/LHC/94-43 LHCC/P1, December 1994;
ATLAS Technical Proposal, CERN/LHC/94-43 LHCC/P2, December 1994.
- [5] G. Bagliesi *et al.*, in Ref. [1], part A.
- [6] S. Moretti, *Z. Phys.* **C75** (1997) 465.

- [7] E. Accomando, A. Ballestrero and M. Pizzio, *Nucl. Phys.* **B512** (1998) 19.
- [8] A. Brandenburg, M. Flesch, P. Uwer, *Phys. Rev.* **D59** (1999) 014001.
- [9] T. Stelzer and W.F. Long, *Comp. Phys. Comm.* **81** (1994) 357;
H. Murayama, I. Watanabe and K. Hagiwara, HELAS: HELicity Amplitude Subroutines for Feynman Diagram Evaluations, *KEK Report* 91-11, January 1992.
- [10] F.A. Berends, P.H. Daverveldt and R. Kleiss, *Nucl. Phys.* **B253** (1985) 441;
R. Kleiss and W.J. Stirling, *Nucl. Phys.* **B262** (1985) 235.
- [11] A. Ballestrero, E. Maina and S. Moretti, *Phys. Lett.* **B335** (1994) 460;
S. Moretti, *Z. Phys.* **C73** (1997) 653;
S. Moretti and K. Odagiri, *Eur. Phys. J.* **C1** (1998) 633;
S. Moretti, *Phys. Rev.* **D50** (1995) 6316.
- [12] JADE Collaboration, *Z. Phys.* **C33** (1986) 23;
JADE Collaboration, *Phys. Lett.* **B213** (1988) 235.
- [13] A. Ballestrero, E. Maina and S. Moretti, *Phys. Lett.* **B333** (1994) 434.
- [14] T. Barklow, P. Chen and W. Kozanecki, in Ref. [1], part A.
- [15] O. Nicrosini and L. Trentadue, *Phys. Lett.* **B196** (1987) 551; *Z. Phys.* **C39** (1988) 479.

$e^+e^- \rightarrow 4 \text{ jets} + \ell^\pm + \cancel{E}$ at the NLC			
σ_{tot} (fb)			
$t\bar{t}$ (NWA)	$t\bar{t} \rightarrow b\bar{b}W^+W^-$	$W^\pm q Q g g$	$W^\pm q Q q' \bar{q}'$
$\sqrt{s} = 360 \text{ GeV}, y_{\ell^\pm, j}^J > 0.003 (M_{ij} > 19 \text{ GeV})$			
76(53)	70(49)	6.5(6.4)	0.42(0.42)
40(28)	37(26)	0.50(0.38)	0.024(0.023)
$\sqrt{s} = 500 \text{ GeV}, y_{\ell^\pm, j}^J > 0.002 (M_{ij} > 22 \text{ GeV})$			
102(99)	102(99)	3.7(3.7)	0.21(0.20)
32(36)	33(36)	0.55(0.32)	0.025(0.019)
$T_{\ell^\pm, j} < 0.75$		$M_{4j} > 0.4\sqrt{s}$	
$\cancel{E} < 0.4\sqrt{s}$		$0.04\sqrt{s} < \vec{p}_{\ell^\pm} < 0.3\sqrt{s}$	
No b -quark tagging			

Table 1: Cross sections of processes (1)–(3), the latter in both NWA and with finite width, at $\sqrt{s} = 360$ and 500 GeV. First line is without the kinematical cuts (8). Second one is with the latter implemented. In brackets, the same rates in presence of Initial State Radiation. A default jet clustering procedure is enforced in all cases.

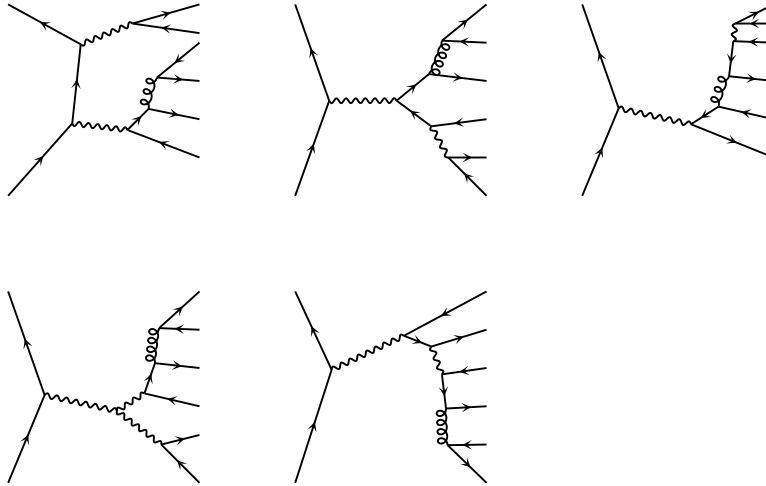


Figure 1: Relevant Feynman sub-diagrams contributing at lowest order to process (1). Permutations of real and virtual lines along the fermion lines are not shown. An internal wavy line represents a W^\pm , a γ or a Z , as appropriate.

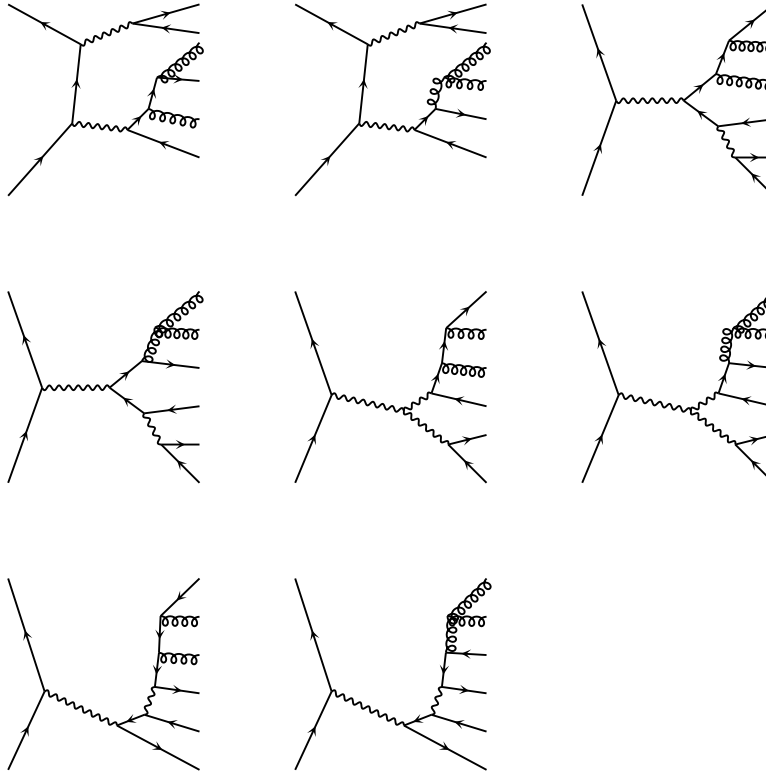


Figure 2: Relevant Feynman sub-diagrams contributing at lowest order to process (2). Permutations of real and virtual lines along the fermion lines are not shown. An internal wavy line represents a W^\pm , a γ or a Z , as appropriate.

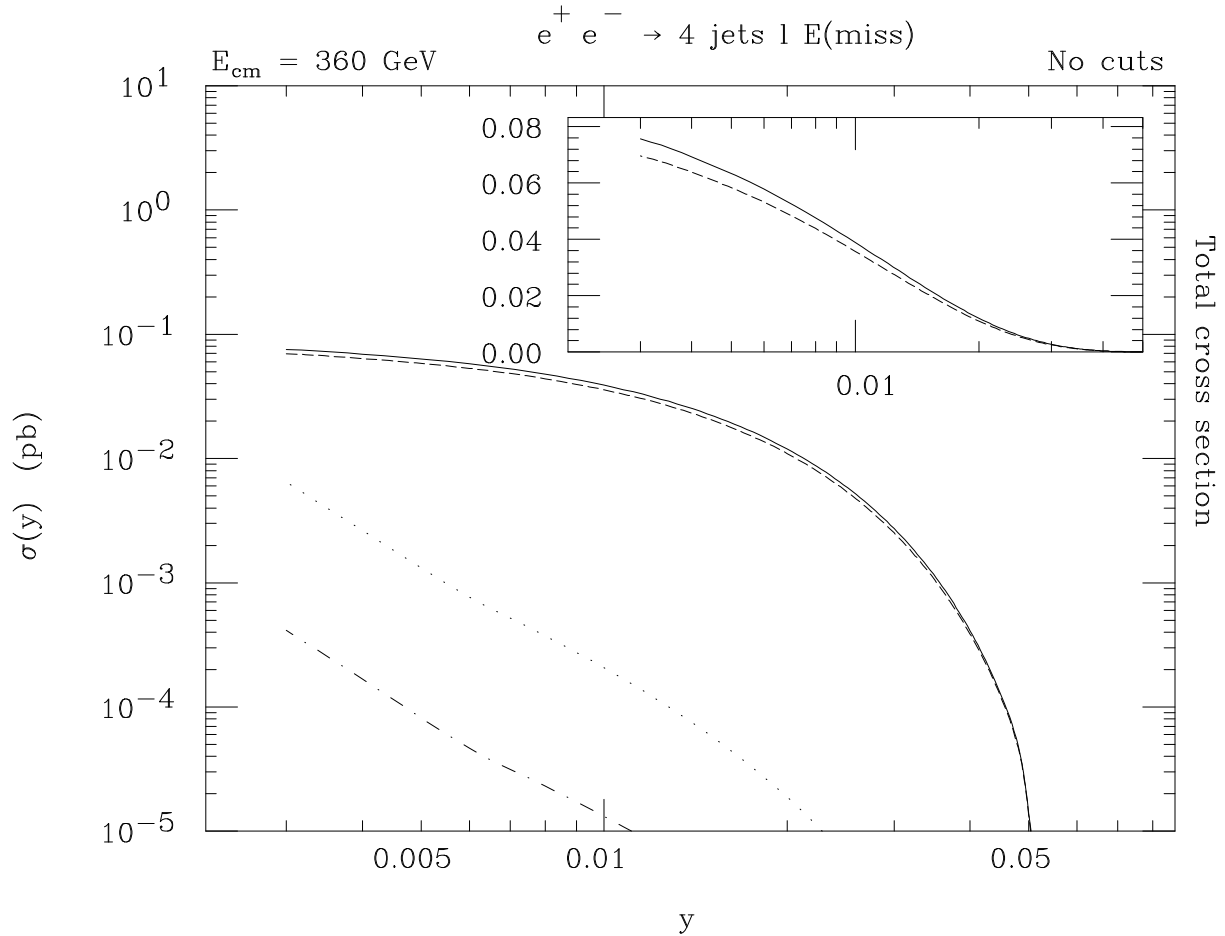


Figure 3: Cross sections of the processes: (3) in NWA (solid) and with finite top width (dashed), (2) (dotted) and (1) (dot-dashed), as a function of y for the Jade algorithm (applied to the four jets and the lepton), at $\sqrt{s} = 360 \text{ GeV}$, before the selection cuts (8) and without ISR. The insert refers to the top-antitop rates only (labelled as above).

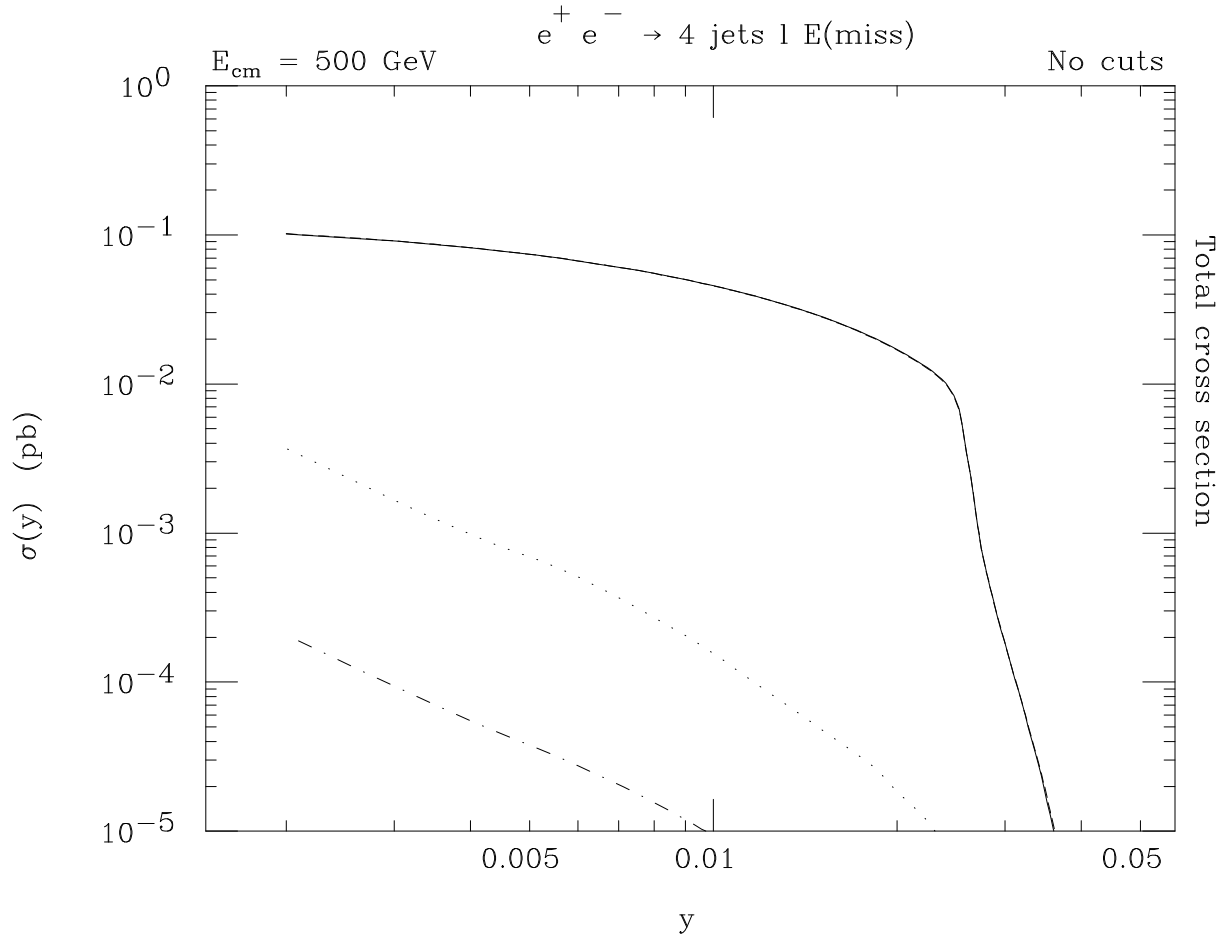


Figure 4: Cross sections of the processes: (3) in both NWA and with finite top width (solid, the two visually coincide), (2) (dotted) and (1) (dot-dashed), as a function of y for the Jade algorithm (applied to the four jets and the lepton), at $\sqrt{s} = 500 \text{ GeV}$, before the selection cuts (8) and without ISR.

$$e^+ e^- \rightarrow 4 \text{ jets } 1 \text{ E(miss)}$$

$$E_{\text{cm}} = 360 \text{ GeV}, y(\text{J}) = 0.003, \text{ cuts}$$

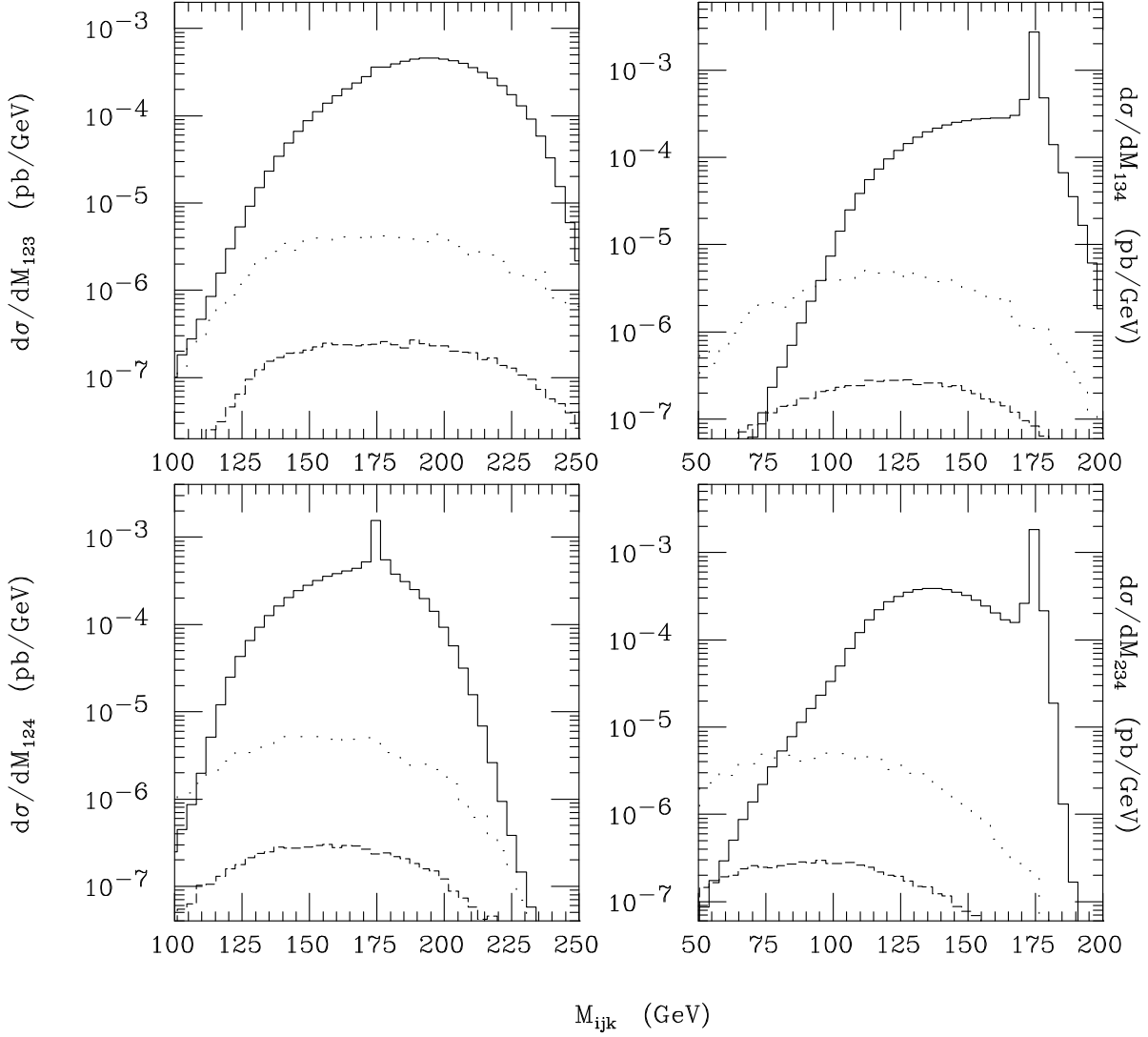


Figure 5: Differential distributions in the invariant mass of the energy-ordered three-jet pairs, M_{ijk} with $i < j < k = 1, \dots, 4$, for the processes: (3) with finite top width (solid), (2) (dotted) and (1) (dashed), for $y = 0.003$ in the Jade algorithm (applied to the four jets and the lepton), at $\sqrt{s} = 360$ GeV. The selection cuts (8) have been enforced and the ISR implemented.

$$e^+ e^- \rightarrow 4 \text{ jets } 1 \text{ E(miss)}$$

$$E_{\text{cm}} = 500 \text{ GeV}, y(\text{J}) = 0.002, \text{ cuts}$$

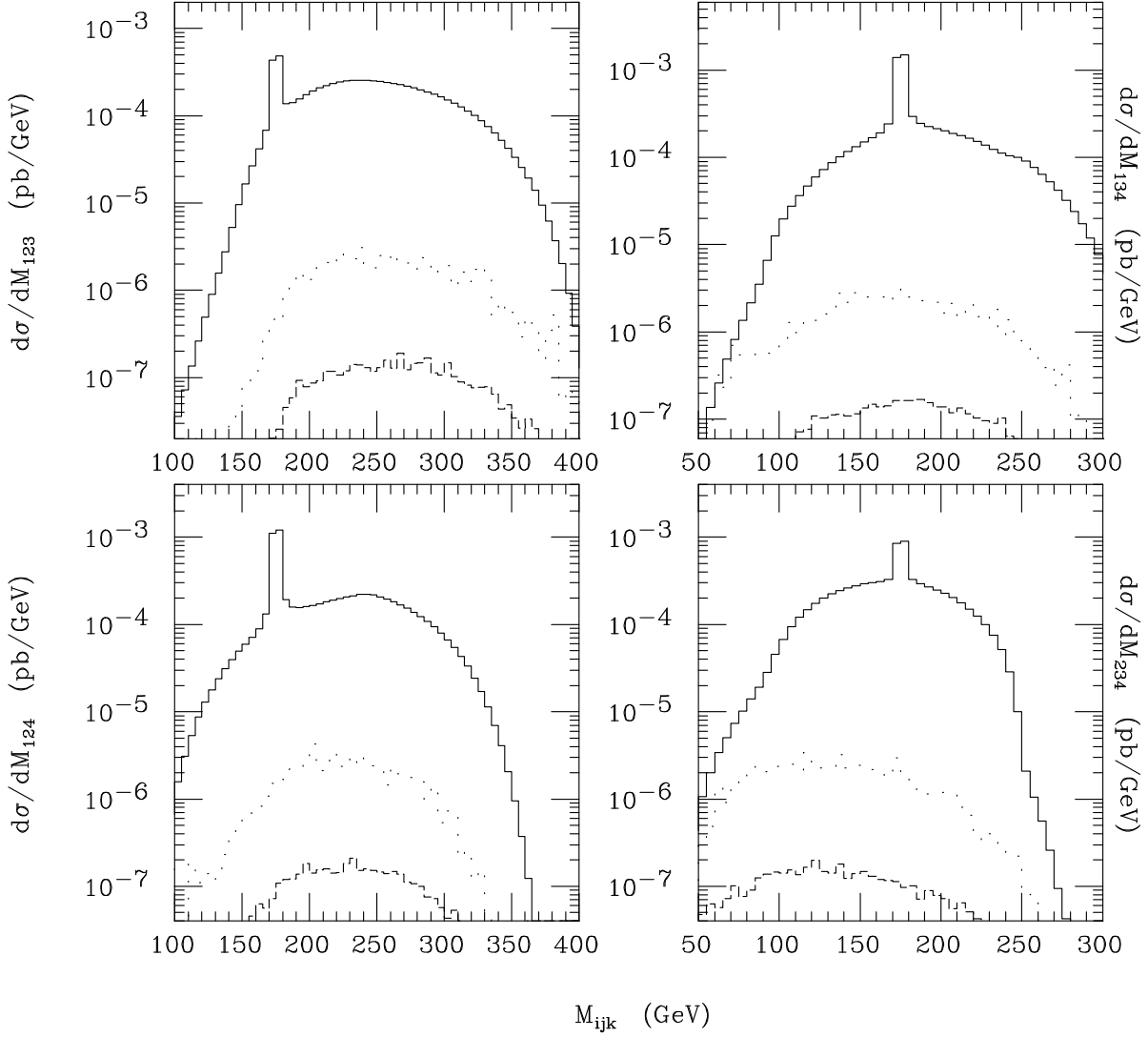


Figure 6: Differential distributions in the invariant mass of the energy-ordered three-jet pairs, M_{ijk} with $i < j < k = 1, \dots, 4$, for the processes: (3) with finite top width (solid), (2) (dotted) and (1) (dashed), for $y = 0.002$ in the Jade algorithm (applied to the four jets and the lepton), at $\sqrt{s} = 500$ GeV. The selection cuts (8) have been enforced and the ISR implemented.

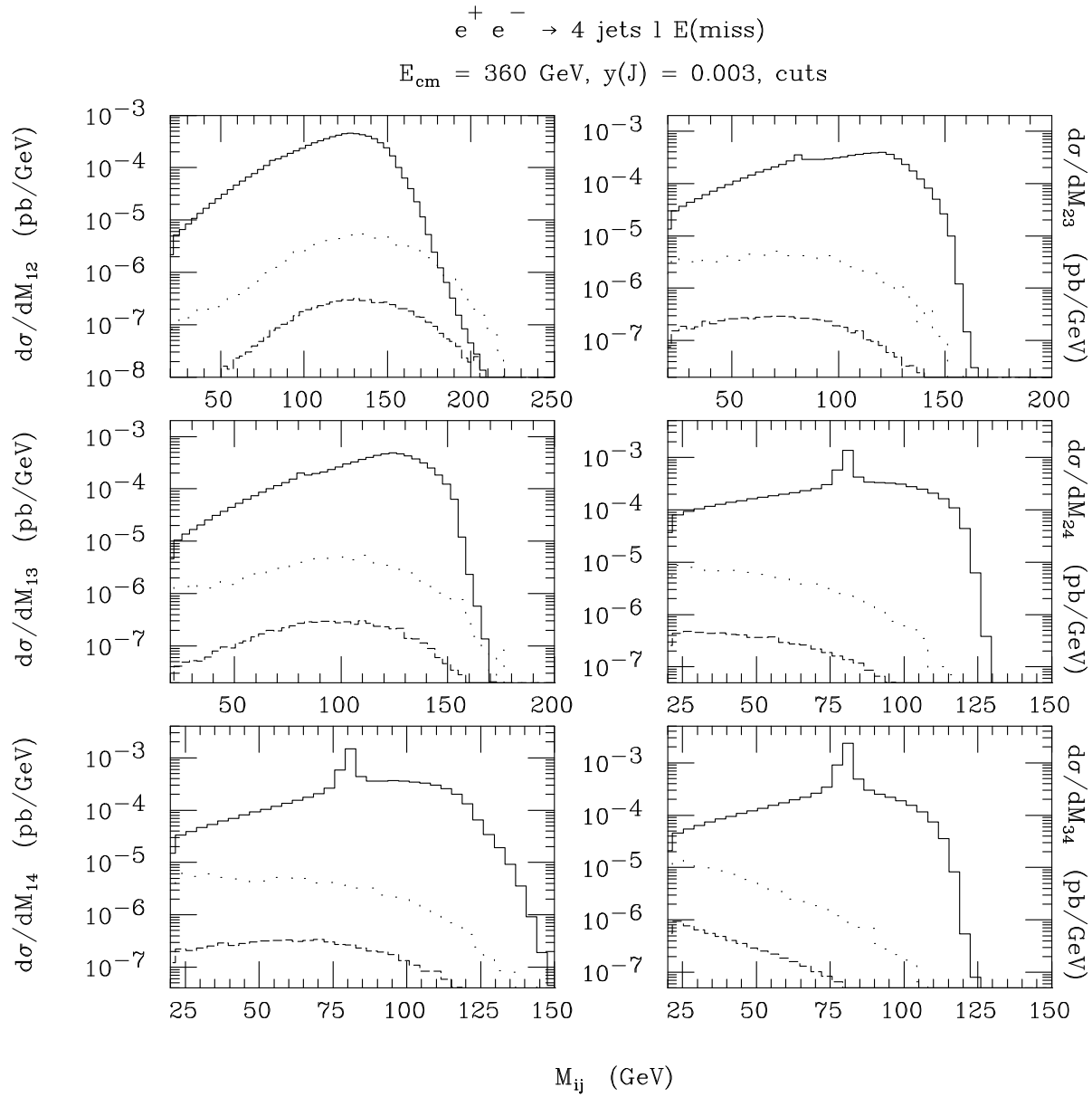


Figure 7: Differential distributions in the invariant mass of the energy-ordered two-jet pairs, M_{ij} with $i < j = 1, \dots, 4$, for the processes: (3) with finite top width (solid), (2) (dotted) and (1) (dashed), for $y = 0.003$ in the Jade algorithm (applied to the four jets and the lepton), at $\sqrt{s} = 360 \text{ GeV}$. The selection cuts (8) have been enforced and the ISR implemented.

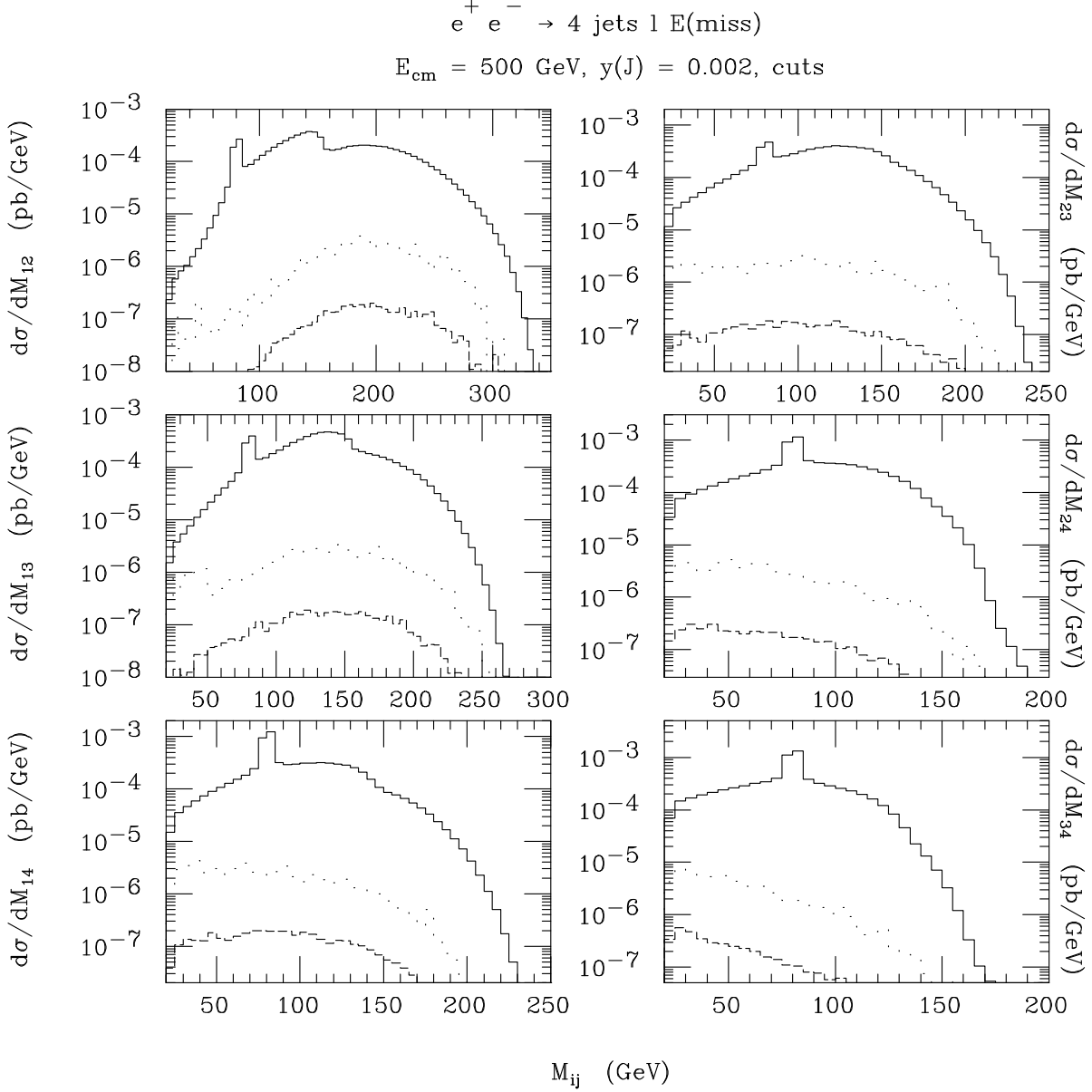


Figure 8: Differential distributions in the invariant mass of the energy-ordered two-jet pairs, M_{ij} with $i < j = 1, \dots, 4$, for the processes: (3) with finite top width (solid), (2) (dotted) and (1) (dashed), for $y = 0.002$ in the Jade algorithm (applied to the four jets and the lepton), at $\sqrt{s} = 500 \text{ GeV}$. The selection cuts (8) have been enforced and the ISR implemented.